Acta Geochim (2026) 45:142–154
https://doi.org/10.1007/s11631-025-00781-y

ORIGINAL ARTICLE

In situ Raman spectroscopic investigation of copper speciation in hydrothermal fluids at temperatures up to 300 °C

Zhenglong Wang[1,2] · Linbo Shang[1] · I-Ming Chou[3] · Chen Chen[1,4] · Yunhe Zhou[1,2] · Jianguo Li[1] · Ziqi Jiang[1] · Xinwei Gao[1,2] · Ye Wan[1]

Received: 3 March 2025 / Revised: 1 April 2025 / Accepted: 10 April 2025 / Published online: 20 May 2025

Abstract The formation of copper deposits is closely related to hydrothermal processes. Understanding the migration of copper in hydrothermal fluids aids in reconstructing mineralization processes and deciphering deposit genesis. Copper primarily exists as Cu^+ and Cu^{2+} in hydrothermal solutions, with redox conditions governing their interconversion. In chloride-rich geological fluids, Cu–Cl complexes are considered critical for copper transport. However, the specific types and valence transitions of Cu–Cl complexes under varying hydrothermal conditions remain poorly understood. This study employed in situ Raman spectroscopy to systematically analyze Cu + HCl and $CuCl_2 + K_2S_2O_3/H_2$ systems under saturated vapor pressure at 25–300 °C, elucidating the effects of temperature, Cl^- concentration, and redox conditions on copper speciation. In the Cu + HCl system, copper dissolved as monovalent Cu–Cl complexes. At high temperatures (> 200 °C), $[CuCl_2]^-$ is the dominated species, whereas $[CuCl_3]^{2-}$ becomes prevalent at lower temperatures and higher HCl concentrations. For the Cu^{2+}–Cl system, the dominant species transitioned from $[Cu(H_2O)_n]^{2+}$ (< 50 °C) to $[CuCl_4]^{2-}$ (100 °C) and further to $[CuCl]^+$ and $[CuCl_2]^0$ at 300 °C. The introduction of reducing agents ($K_2S_2O_3/H_2$) facilitated $Cu^{2+} \rightarrow Cu^+$ reduction, thereby stabilizing Cu^+–Cl complexes and inducing partial copper precipitation. The behavior of copper in chloride-rich hydrothermal fluids observed in this study indicates that high-temperature oxidizing fluids facilitate Cu mobilization, while cooling and redox changes promote deposition and ore minerals formation.

Keywords Raman spectroscopy · In situ analysis · Hydrothermal fluids · Copper · Transport mechanism

1 Introduction

Global copper deposits (e.g., porphyry, sediment-hosted, IOCG, epithermal) are closely associated with hydrothermal systems. Studies indicate that copper in hydrothermal fluids exists in two oxidation states, Cu^+ and Cu^{2+}, and migrates

✉ Linbo Shang
shanglinbo@vip.gyig.ac.cn

Zhenglong Wang
wangzhenglong@mail.gyig.ac.cn

I-Ming Chou
imchou@idsse.ac.cn

Chen Chen
chenchen@cdut.edu.cn

Yunhe Zhou
zhouyunhe@mail.gyig.ac.cn

Jianguo Li
lijianguo@mail.gyig.ac.cn

Ziqi Jiang
jiangziqi@mail.gyig.ac.cn

Xinwei Gao
gaoxinwei@mail.gyig.ac.cn

Ye Wan
wanye@mail.gyig.ac.cn

[1] State Key Laboratory of Critical Mineral Research and Exploration, Institute of Geochemistry, Chinese Academy of Sciences, Guiyang 550081, China

[2] University of Chinese Academy of Sciences, Beijing 100049, China

[3] Institute of Deep-Sea Science and Engineering, Chinese Academy of Sciences, Sanya 572000, China

[4] State Key Laboratory of Oil and Gas Reservoir Geology and Exploitation, Chengdu University of Technology, Chengdu 610059, China

primarily as Cu–Cl complexes. The stability of these complexes directly governs copper solubility and transport capacity, thereby controlling mineralization processes. Therefore, understanding the speciation of Cu–Cl complexes in hydrothermal fluids and their controlling factors is critical for deciphering copper migration, precipitation, and the hydrothermal alteration and overprinting of copper deposits (Liu et al. 2002; Hua et al. 2004; Brugger et al. 2007; Zhang et al. 2021).

Previous studies utilizing experimental approaches such as solubility experiments, UV-Vis spectroscopy, and x-ray absorption spectroscopy (XAS) have both inferred and observed in situ the migration forms of copper in hydrothermal fluids. Results indicate that $[Cu(H_2O)]^+$, $[CuCl]^0$, and $[CuCl_2]^-$ are the dominant species in low-Cl^-, reduced fluids (Xiao et al. 1998; Liu et al. 2001). With increasing chloride concentration, higher-order complexes such as $[CuCl_3]^{2-}$ become more prevalent, and even $[CuCl_4]^{3-}$ may form (Liu et al. 2002; Berry et al. 2006). However, some studies argue that $[CuCl_4]^{3-}$ remains unstable in aqueous solutions (Brugger et al. 2007; Sherman 2007). As temperature rises, the stability of other chloride species decreases, whereas $[CuCl_2]^-$ becomes increasingly stable (Xiao et al. 1998; Liu et al. 2002; Brugger et al. 2007). Both chloride concentration and temperature critically influence the stability of Cu–Cl complexes, thereby controlling copper solubility in hydrothermal fluids. Thermodynamic modeling reveals that a decrease in chloride concentration from 5 to 1 m (molality, mol/kg H_2O) at 300 °C reduces dissolved copper concentration by 90% (Liu et al. 2002). Similarly, cooling from 350 to 250 °C leads to approximately 90% copper precipitation (Xiao et al. 1998). Investigating the effects of chloride concentration and temperature on copper transport mechanisms is fundamental for reconstructing mineralization processes and deciphering deposit genesis.

In near-surface highly oxidizing environments, copper primarily exists as Cu^{2+}–Cl complexes, which play a critical role in the formation of supergene enrichment zones in mineral deposits (Rickard and Cowper 1994; Hua et al. 2004). Under high-chloride conditions, Cu^{2+} can form various chloride species, such as $[CuCl]^+$, $[CuCl_2]^0$, $[CuCl_3]^-$, and $[CuCl_4]^{2-}$. Due to the high solubility of Cu^{2+}–Cl complexes in hydrothermal solutions, changes in their speciation are generally considered unrelated to copper precipitation. UV–Vis-NIR spectroscopy and XAS studies suggest that $[CuCl_4]^{2-}$ and $[CuCl_2(OH_2)_4]^0$ may be the most significant complexes in oxidized brines associated with mineralization (Collings et al. 2000; Brugger et al. 2001). Solubility experiments further indicate that Cu^{2+} exhibits higher solubility, highlighting the importance of redox transitions between Cu^+ and Cu^{2+} in controlling copper transport and deposition (Berger and Winand 1984; Jianu et al. 2018). X-ray absorption near-edge structure (XANES) spectroscopy analyses of natural fluid inclusions suggest that Cu^+ may oxidize to Cu^{2+} under acidic and low-temperature conditions, a process interpreted as a temperature-dependent reversible redox reaction (Mavrogenes et al. 2002; Berry et al. 2006, 2009). However, an alternative hypotheses proposed that transitions between Cu^+ and Cu^{2+} in the same system could result from artifacts induced by x-ray beam exposure during analysis (Brugger et al. 2007). Despite these insights, systematic studies on Cu speciation under redox fluctuations in hydrothermal systems remain scarce.

Laser Raman spectroscopy combined with visualized experimental setups can provide in situ spectroscopic information on copper complexes in fluids. By integrating with fused silica capillaries, real-time monitoring of system states during heating–cooling cycles is achievable. Applegarth et al. (2014) analyzed the CuCl + 6 m HCl system at 25–80 °C using Raman spectroscopy and ab initio calculations, identifying $[CuCl_2]^-$ and $[CuCl_3]^{2-}$ as the dominant complexes, with corresponding Raman peaks at 297 ± 3 cm^{-1} and 247 ± 3 cm^{-1}, respectively. Schmidt et al. (2018) conducted Raman studies on CuS/Cu mixed with NaCl/HCl systems under high-temperature and high-pressure conditions (300–600 °C, 2 GPa), revealing $[CuCl_2]^-$ as the primary species, and $[CuCl_3]^{2-}$ at high HCl concentrations (5 m), with $[CuCl_2]^-$ peaks at 280–290 cm^{-1} and $[CuCl_3]^{2-}$ peaks near 250 cm^{-1}. The observed peak shifts compared to Applegarth et al. (2014) were attributed to temperature effects. For Cu^{2+}–Cl complexes, systematic Raman studies remain limited. Scholars hypothesize their Raman peaks lie within 200–340 cm^{-1} (Tanimizu et al. 2007; Yang and Xu 2011; Wu et al. 2016). To further investigate the evolution of Cu–Cl speciation under varying temperature (25–300 °C), chlorine concentration (1–6 m), and redox conditions ($H_2/K_2S_2O_3$-controlled systems), this study employs an *in situ* Raman analysis system coupled with fused silica capillaries. Through meticulous spectral analysis, the effects of chloride concentration, temperature, and redox conditions on copper transport mechanisms in hydrothermal fluids are elucidated.

2 Experimental

2.1 Sample chamber

2.1.1 FSCC

For experiments without hydrogen addition, FSCC (fused silica capillary capsule) developed by Chou et al. (2008) was employed as the sample chamber for spectroscopic analysis (Fig. 1a). The FSCC specifications were as follows: inner diameter of 150 μm, outer diameter of 665 μm, and length ≤ 2 cm. A 4-cm-long fused silica capillary capsule

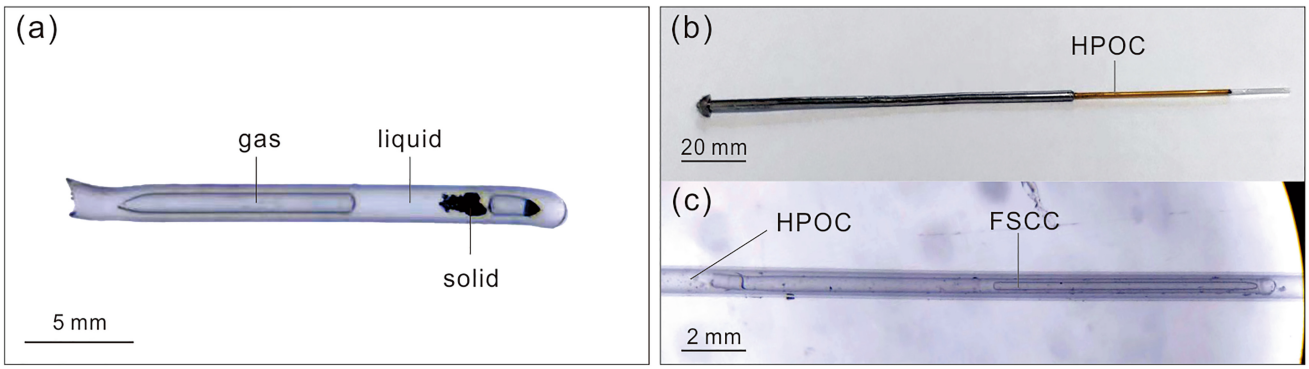

Fig. 1 FSCC sample chamber (**a**); exterior (**b**) and interior (**c**) of FSCC and HPOC combined chamber

was cut using a ceramic blade. The brown polyimide coating on the surface was removed by flame treatment with an alcohol lamp. One end of the capillary was sealed using a hydrogen–oxygen flame. After heating the tube wall, the open end was immersed in a pre-prepared solution to draw the liquid into the capillary during cooling. Solid powders were added by directly inserting the open end into the powder. After each addition of solutions or solid, the capillary was centrifuged to move the sample toward the sealed end. Then, the open end was connected to the vacuum pump, and the sealed end was immersed in liquid nitrogen to freeze the solution, followed by vacuum evacuation using a vacuum pump. The other end was subsequently sealed with a hydrogen–oxygen flame. The fully sealed capillary was placed on a heating-cooling stage, and Raman spectra were collected during temperature cycling. To ensure complete reaction of solid samples, the system was heated to 350 °C and held for ≥ 4 h until gas generation ceased. During cooling, Raman spectra were collected at the set temperatures after allowing the system to equilibrate for ≥ 2 h.

2.1.2 FSCC and HPOC combined chamber

For experiments involving hydrogen addition, a combined FSCC and HPOC (high-pressure optical cell) system developed by Chou et al. (2021) was employed (Fig. 1b, c). The fused silica capillaries used for FSCC preparation had specifications of inner diameter 150 μm, outer diameter 365 μm, and length ≤ 2 cm. For HPOC fabrication, capillaries with an inner diameter of 450 μm, outer diameter of 670 μm, and length ≈15 cm were selected. A 15-cm-long capillary (HPOC specifications) was cut using a ceramic blade. Approximately 2 cm of the brown polyimide coating was removed by flame treatment with an alcohol lamp. The FSCC was then inserted into the HPOC, and one end of the HPOC was sealed using a hydrogen–oxygen flame. The other end was coated with high-pressure epoxy resin adhesive and sleeved with a 10-cm-long stainless steel tube. The stainless steel end of the HPOC was connected to the gas line, while the opposite end was placed on a heating-cooling stage. After heating to the target temperature, the system was held for ≥ 4 h to stabilize the sample. Real-time internal changes were monitored through the transparent fused silica capillary under a microscope, while Raman spectra were simultaneously collected.

2.2 Sample solutions

The initial samples for the experiments in this study were prepared using chemical reagents, including metallic copper powder (Cu, 99.9% metal basis, Shanghai Aladdin Biochemical Technology Co., Ltd.), copper chloride ($CuCl_2 \cdot 2H_2O$, analytical grade, Tianjin Ruijinte Chemical Co., Ltd.), hydrochloric acid (HCl, guaranteed reagent, GR, Sinopharm Chemical Reagent Co., Ltd.), potassium thiosulfate ($K_2S_2O_3$, analytical grade, purity 99.9%, Shanghai Aladdin Biochemical Technology Co., Ltd.), and deionized water. The concentration units of all solutions were expressed in molality. The components/compositions of the prepared sample solutions are shown in Table 1.

Table 1 Initial sample components/compositions

Solid	HCl (mol/kg)	$CuCl_2$ (mol/kg)	$K_2S_2O_3$ (mol/kg)	Gas
Cu	1.0	–	–	–
Cu	2.0	–	–	–
Cu	3.0	–	–	–
Cu	6.0	–	–	–
–	–	0.47	0.1	–
–	–	1.0	–	H_2

2.3 Raman spectral collection and calibration

The Raman spectroscopic analyses were conducted at the State Key Laboratory for Critical Mineral Research and Exploration using a LabRAM HR Evolution Raman spectrometer (JY Horiba) equipped with 5×, 10×, 20×, and 50× microscope objectives. The laser spot diameter was approximately 2 μm, with a spectral collection range of 100–4200 cm^{-1} and a grating resolution of 600 g/mm. A 532.17-nm laser was used for excitation. To ensure consistency in Raman intensity comparisons across samples, identical acquisition conditions were applied: laser power at 100 mW, integration time of 30 s, and ≥3 accumulations. Temperature was controlled using a Linkam CAP500 heating-cooling stage, the temperature was previously calibrated with the triple points of H_2O (0.0 °C), CO_2 (−56.6 °C), and the melting point of $NaNO_3$ (306.8 °C), and the reported temperature is accurate to ±0.1 °C. Hydrogen pressure within the HPOC was monitored via a Setra 204D pressure transducer and displayed on a Datum 2000™ digital pressure gauge (maximum detectable pressure: 0.69 MPa, accuracy ± 0.14%).

Prior to spectral collection, the spectrometer was calibrated using v_1 peak of a silicon wafer (520.7 cm^{-1}) as an external standard. During experiments, neon lamp emission lines (2209.35, 2330.40, 2389.35, 2514.58, 2568.81, and 2708.91 cm^{-1}) were collected as internal standards for spectral calibration. Acquired spectra were processed using PeakFit and Origin software, with Gaussian functions applied to peak fitting. The experimental setup is illustrated in Fig. 2.

Hydrogen was introduced into the system as follows: First, the vacuum pump was activated to evacuate gases until the internal pressure of the HPOC was reduced to < 0.01 MPa. Then, the high-pressure valve of the hydrogen tank was opened to introduce hydrogen into the HPOC. Gas diffusion through the fused silica capillary equilibrates hydrogen between the FSCC and the HPOC (Chou et al. 2021). The internal hydrogen pressure of the HPOC (~0.24 MPa during experiments) was measured using a pressure gauge.

3 Results

3.1 Effect of HCl concentration

In the Cu + HCl system, Raman spectra were collected in situ after the reaction reached equilibrium. As shown in Fig. 3, distinct Raman peaks at 235, 297, and 4156 cm^{-1} are observed at 150 °C and 250 °C, indicating the formation of Cu–Cl complexes and hydrogen gas (H_2) through reactions between Cu and HCl (Schmidt et al. 2018).

The Raman peaks in the 200–300 cm^{-1} range are attributed to Cu–Cl stretching vibration (Applegarth et al. 2014; Schmidt et al. 2018). Peak fitting of Raman spectra for the Cu + 3 m HCl system at 150 °C reveals two peaks at

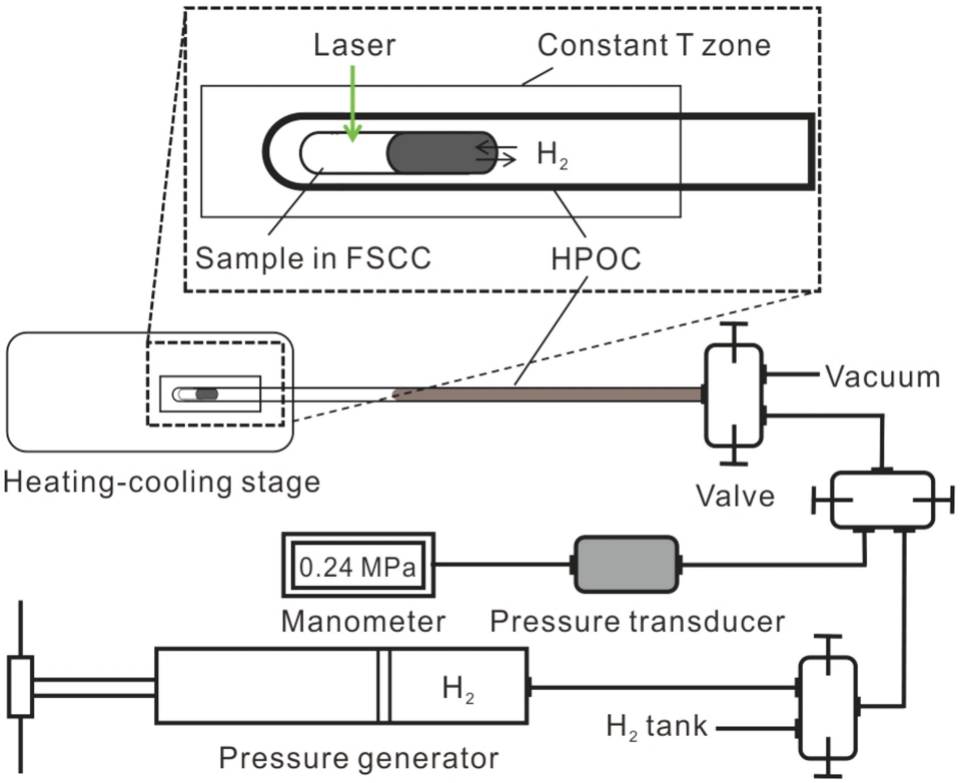

Fig. 2 Schematic diagram of the experimental setup, modified from Chou et al. (2021)

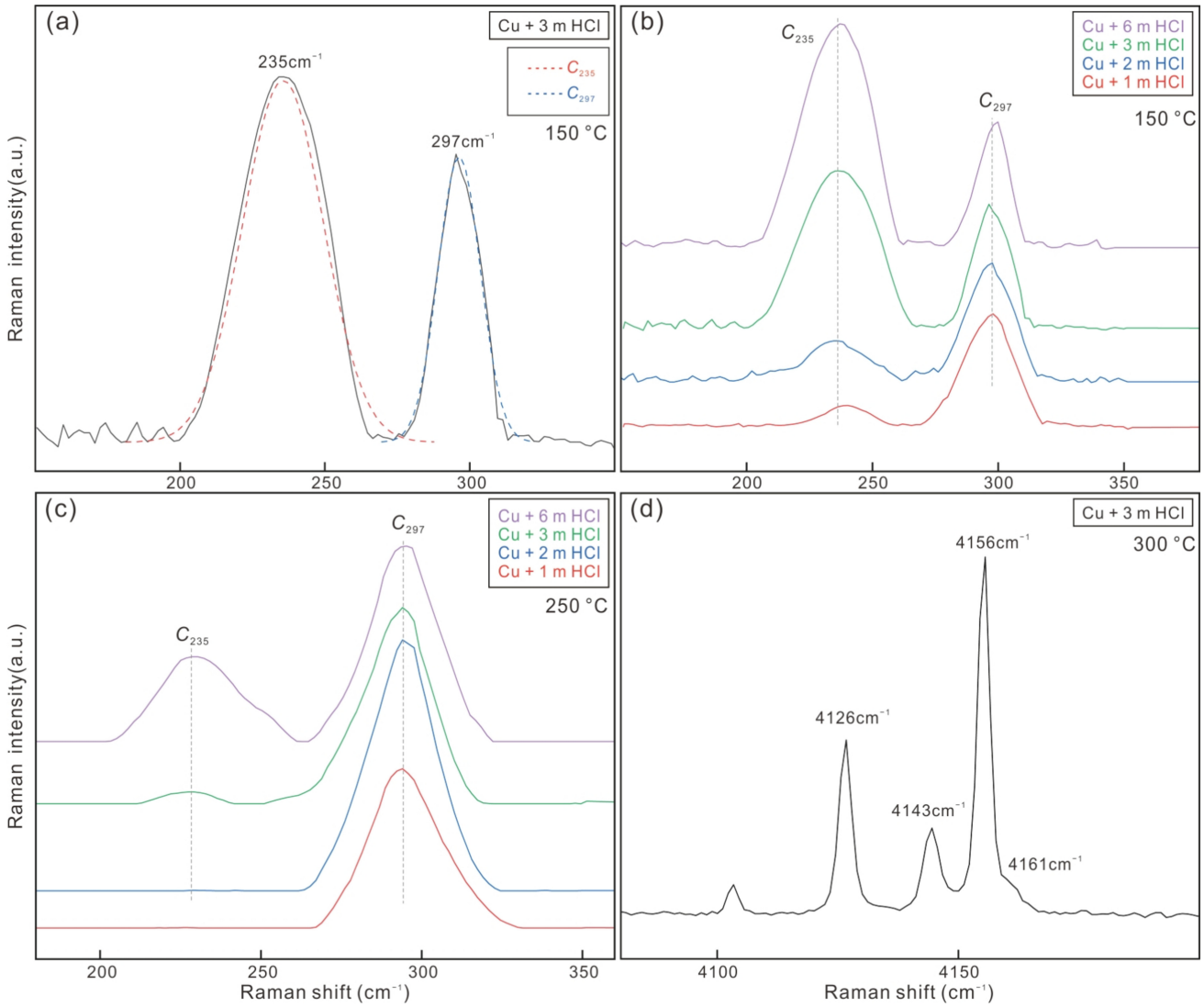

Fig. 3 Raman spectra of Cu+HCl systems. **a** Peak fitting of Cu–Cl stretching region; **b** 150 °C; **c** 250 °C; **d** vibrational bands of H_2

235 cm^{-1} (C_{235}) and 297 cm^{-1} (C_{297}) (Fig. 3a), with a confidence level of 99%. At 150 °C, Raman spectra of solutions with varying HCl concentrations (1–6 m HCl) exhibit two prominent peaks at 235 cm^{-1} and 297 cm^{-1}. As HCl concentration increases, the intensity of C_{235} significantly increases, while the relative intensity of C_{297} decreases (Fig. 3b). At 250 °C, the Raman spectra for 1–6 m HCl solutions show a dominant peak at 297 cm^{-1}, with a higher-intensity C_{235} being observed only in 6 m HCl solution (Fig. 3c). Additionally, at 300 °C, characteristic Raman peaks at 4126, 4143, 4156, and 4161 cm^{-1} are detected in Cu solutions with different HCl concentrations (Fig. 3d), corresponding to vibrational bands of dissolved H_2 (aq) (Stoicheff 1957).

3.2 Effect of temperature

The Cu + HCl system reached equilibrium after reacting at 350 °C for 4 h. During the cooling process, in situ Raman spectra were collected from 300 to 24 °C (Fig. 4a–c). The Raman spectra reveal that the species represented by Peaks C_{235} and C_{297} are the main components in the solution. The Raman intensity of C_{235} is strongest at room temperature and gradually decreases with temperature increases, accompanied by its peak position shifts to lower wavenumbers. Comparative analysis shows that higher HCl concentrations enable detection of C_{235} at elevated temperatures: in 2 m and 3 m HCl solutions, the maximum detectable temperatures for C_{235} are 150 °C and 200 °C respectively, while in 6 m HCl solution, C_{235} remains detectable even at 300 °C. Conversely, the Raman intensity of C_{297} progressively increases

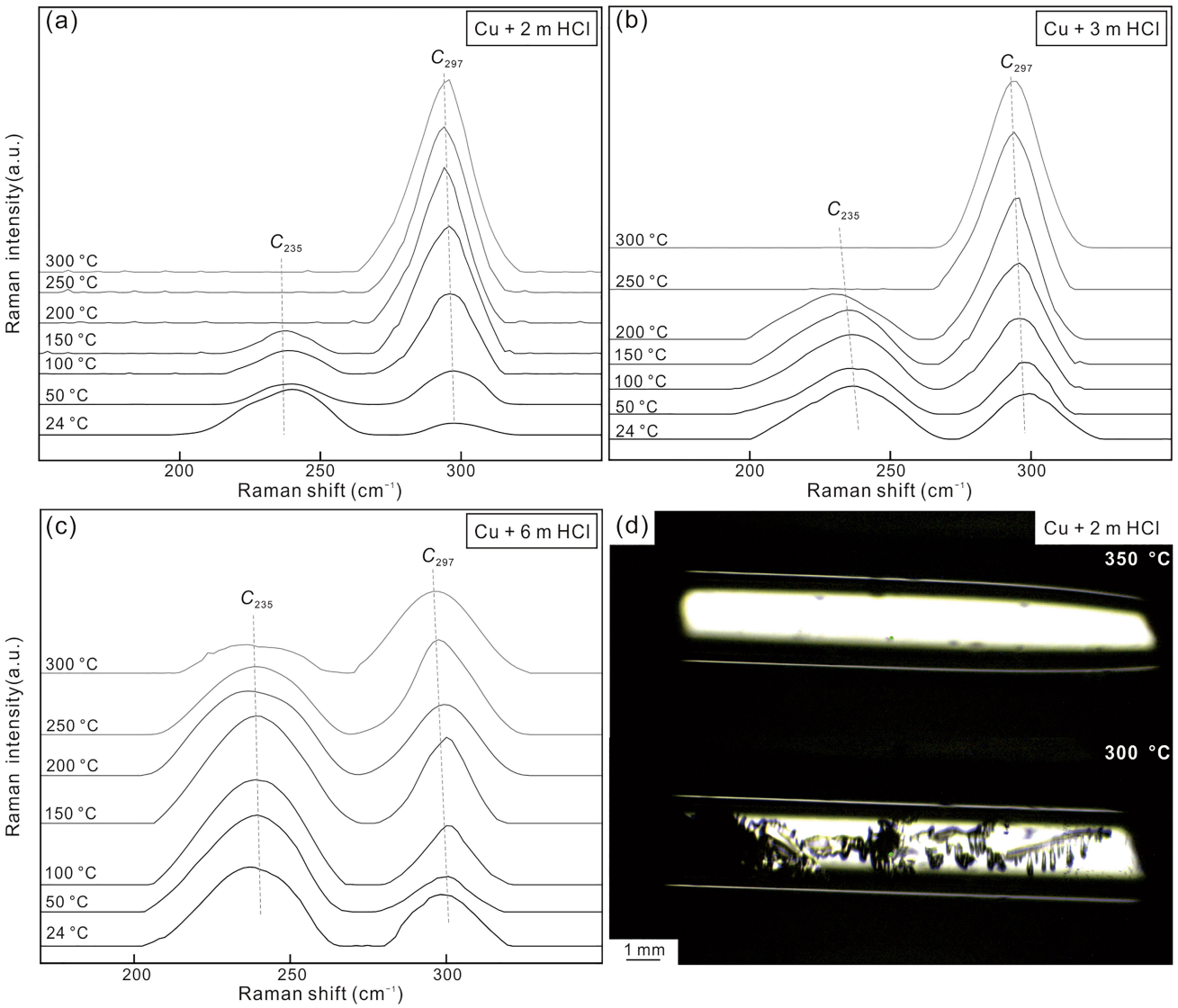

Fig. 4 Raman spectra and microscopic images at 24–350 °C. **a** Raman spectra of Cu + 2 m HCl; **b** Raman spectra of Cu + 3 m HCl; **c** Raman spectra of Cu + 6 m HCl; **d** microscopic images of Cu + 2 m HCl

with rising temperature and reaches maximum intensity at 300 °C, accompanied by a gradual low-wavenumber shift of its peak position.

In addition to spectral collection, real-time microscopic observations were conducted during cooling (Fig. 4d). When the temperature of the Cu + 2 m HCl system decreases from 350 to 300 °C, transparent crystalline precipitates form in the solution, with continuous crystal accumulation observed during further cooling. Attempts to collect Raman spectra from the crystals are unsuccessful due to their thermal instability: minor laser-induced temperature fluctuations cause crystal melting. Based on system components (H^+, Cu^+, Cl^-), the crystals are speculated to be solid CuCl precipitates formed by decreased copper solubility at lower temperatures.

3.3 Effect of redox conditions

3.3.1 H_2 system

The 1 m $CuCl_2$ solution was heated to 300 °C, and hydrogen gas was introduced by opening the hydrogen valve under a pressure of 0.24 MPa. In situ Raman spectra and microscopic images were collected before and after hydrogen addition (Fig. 5a–c). After the system had been completely reduced by H_2, the FSCC was removed, reheated to 300 °C, and held for 24 h. Raman spectra were then collected during the cooling process (Fig. 5d). Concurrent microscopic observations revealed a color change in the solution after H_2 introduction: transitioning from the yellow characteristic of

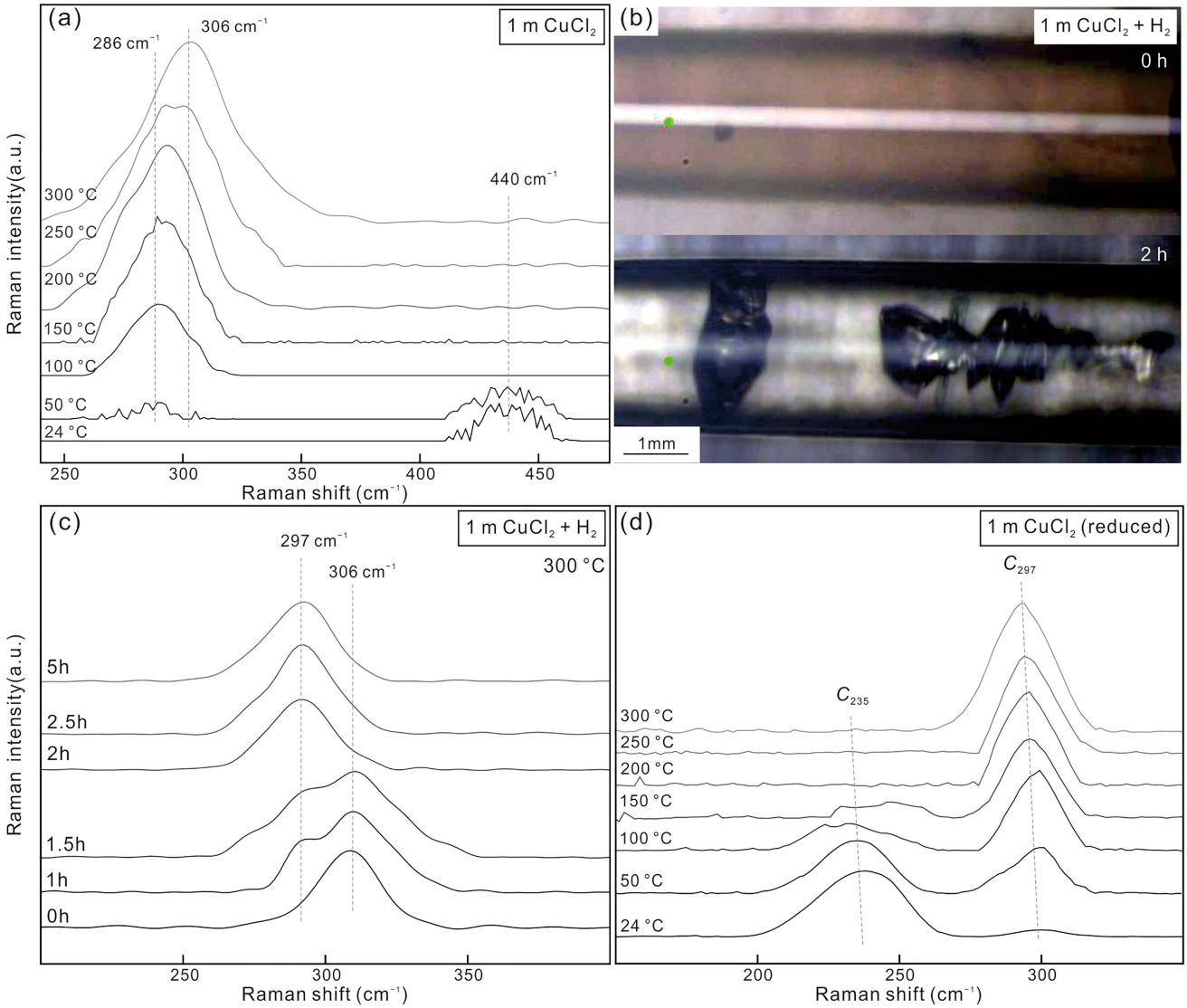

Fig. 5 **a** Raman spectra of 1 m $CuCl_2$ system at 24–300 °C; **b** microscopic images were obtained for 1 m $CuCl_2$ system both before and after 2 h of H_2 exposure; **c** Raman spectra were monitored during continuous hydrogen introduction at 300 °C, with the pressure of H_2 maintained at 0.24 MPa in the HPOC. **d** The 1 m $CuCl_2$ system was fully reduced by H_2, followed by reheating at 300 °C for 24 h without H_2, and then the Raman spectra were collected during the cooling process

Cu^{2+}–Cl solutions to the colorless appearance of Cu^{+}–Cl solutions (Scholz et al. 1972; Applegarth et al. 2014).

As shown in Fig. 5a, the 1-m $CuCl_2$ system exhibits only a weak Raman peak at 440 cm^{-1} at room temperature. Upon heating to 50 °C, a new Raman peak emerges at 286 cm^{-1}. With increasing temperature, the peak position gradually shifts to higher wavenumbers, reaching 306 cm^{-1} at 300 °C, accompanied by a light yellow solution color in the microscopic image (Fig. 5b). Then, hydrogen gas was introduced into the system and diffused into the inner tube with $CuCl_2$ solution. As shown in Fig. 5c, during the first 1–1.5 h of hydrogen introduction, a new Raman peak at 297 cm^{-1} appears alongside the 306 cm^{-1} peak. After 2 h of hydrogen exposure, the 306 cm^{-1} peak completely disappears, leaving only the 297 cm^{-1} peak. Microscopic observations show a colorless solution with simultaneous precipitation of transparent crystals, hypothesized to be CuCl solids (Fig. 5b). The temperature-dependent Raman spectra of 1 m $CuCl_2$ system reduced by hydrogen gas (Fig. 5d) exhibit behavior similar to the Cu + HCl system, only the C_{297} peak is observed above 200 °C, while both C_{297} and C_{235} peaks appear below 200 °C. The Raman intensity of C_{235} increases with decreasing temperature, whereas C_{297} intensity intensifies with rising temperature.

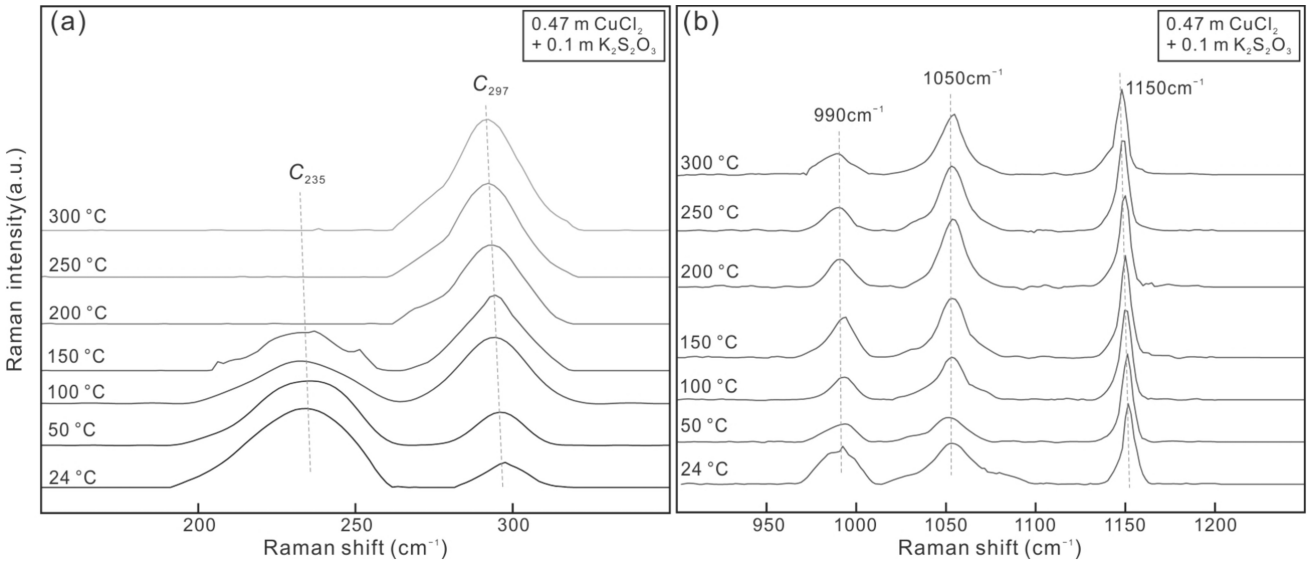

Fig. 6 Raman spectra of $CuCl_2 + K_2S_2O_3$ system were collected during the cooling process in 300–24 °C after complete reaction at 350 °C. **a** Cu–Cl stretching region; **b** S–O stretching region

3.3.2 $K_2S_2O_3$ system

The 0.47 m $CuCl_2 + 0.1$ m $K_2S_2O_3$ system, after complete reaction at 350 °C, underwent Raman spectral collection during cooling (Fig. 6). Similar to experiments with the $CuCl_2 + H_2$ system, the thermal decomposition of $K_2S_2O_3$ at elevated temperatures facilitates the reduction of Cu^{2+} to Cu^+. Above 200 °C, only C_{297} is observed, while both C_{297} and C_{235} are detected below 200 °C (Fig. 6a). Simultaneously, Raman spectra in the 900–1200 cm^{-1} region (Fig. 6b), associated with S–O vibrational modes, reveal sulfur-containing species including SO_4^{2-} (980–990 cm^{-1}), HSO_4^- (1050 cm^{-1}), and SO_2 (1150 cm^{-1}) (Hurai et al. 2015). Notably, no H_2S-related Raman peaks near 2600 cm^{-1} are observed (Hurai et al. 2015), indicating the predominance of oxidized sulfur species in the post-reaction system. This further confirms that the reduction of sulfur species facilitates the conversion of Cu^{2+} to Cu^+.

Table 2 Previously reported Raman shifts of copper-chloride and copper-aquo complexes

Oxidation state	Species	Raman shift (cm^{-1})	Source	This article's data (cm^{-1})
Cu^+	$[Cu(H_2O)_n]^+$	370	Fujii et al. (2013)	
		410 (speculation)	Applegarth et al. (2014)	
	$[CuCl(H_2O)]^0$	350, 410 (speculation)	Applegarth et al. (2014)	
	$[CuCl_2]^-$	280–290	Schmidt et al. (2018)	297
		296	Creighton and Lippincott (1963)	
		297 ± 3	Applegarth et al. (2014)	
		300	Axtell et al. (1973)	
	$[CuCl_3]^{2-}$	247 ± 3	Applegarth et al. (2014)	235
		~250	Schmidt et al. (2018)	
Cu^{2+}	$[Cu(H_2O)_n]^{2+}$	436	Davis and Chong (1972)	440
		440	Hester and Planes (1964)	
	$[CuCl]^+$, $[CuCl_2]^0$	200–340 (speculation)	Wu et al. (2016)	306 (speculation)
	$[CuCl_4]^{2-}$	280 (speculation)	Tanimizu et al. (2007)	286 (speculation)
		286 (speculation)	Yang and Xu (2011)	
	$[CuCl_6]^{4-}$	286 (speculation)	Yang and Xu (2011)	

4 Discussion

4.1 Component attribution

The analysis here primarily focuses on the Cu-Cl or Cu-O vibrational spectral region associated with copper complexes within the 200–500 cm^{-1} range. Table 2 summarizes previously reported Raman shifts of copper-chloride or copper-hydroxide complexes.

4.1.1 Monovalent copper (Cu^+) species

Studies employing solubility method, UV–Vis spectrophotometry, and XAS indicate that the $[CuCl_2]^-$ complex predominates under conditions of relatively low chloride concentrations and elevated temperatures, with its stability increasing progressively at higher temperatures (Xiao et al. 1998; Liu et al. 2002; Brugger et al. 2007). As summarized in Table 2, Raman studies of $[CuCl_2]^-$ identify its characteristic v_1 symmetric Cu–Cl stretching vibration at approximately 300 cm^{-1} under ambient conditions (Creighton and Lippincott 1963; Axtell et al. 1973; Applegarth et al. 2014), with potential low-wavenumber shifts observed under high-temperature, high-pressure conditions (Schmidt et al. 2018). In the Cu + HCl system studied in this work, the Raman intensity and peak area of C_{297} increase with rising temperatures and decreasing HCl concentration (Fig. 4a–c), indicating that the species represented by C_{297} is dominant in the solution under higher temperatures and lower HCl concentrations. Therefore, C_{297} is conclusively assigned to the v_1 symmetric Cu–Cl stretching vibration of $[CuCl_2]^-$ complex in this study.

Liu et al. (2002) using UV-Vis spectrophotometry, proposed that higher-order complexes like $[CuCl_4]^{3-}$ replace $[CuCl_3]^{2-}$ with increasing chloride concentration. Brugger et al. (2007) demonstrated through XAS study that the $[CuCl_3]^{2-}$ complex dominates under high-salinity and low-temperature conditions. Applegarth et al. (2014) supported this conclusion via Raman spectroscopy, observing that $[CuCl_3]^{2-}$ becomes increasingly predominant with decreasing temperature and rising HCl concentration. They assigned the Raman peak at 247 cm^{-1} to the v_1 symmetric Cu–Cl stretching vibration of $[CuCl_3]^{2-}$. In our experiment, C_{235} is observed in 1–6 m HCl solutions at 25–300 °C. At constant HCl concentration, the Raman intensity and peak area of C_{235} increase progressively with cooling and stabilize (Fig. 4a–c). At 150 °C and 250 °C, higher HCl concentrations further amplify the Raman intensity of C_{235} (Fig. 3b, c), showing greater dominance at lower temperatures (150 °C). Aligning with previous findings, the relative abundance of the C_{235}-associated species grows with decreasing temperature and rising chloride concentration. Thus, we assign C_{235} to the $[CuCl_3]^{2-}$ complex. The observed discrepancy between our peak position (235 cm^{-1}) and Applegarth et al.'s (2014) reported 247 cm^{-1} for $[CuCl_3]^{2-}$ may arise from challenges in baseline selection caused by weak Raman intensity in their experiments. Liu et al. (2002) proposed that UV-Vis spectral changes in solution with Cl^- concentrations > 6 m under high-temperature conditions (200–300°C) originate from the fomation of the higher-order complex $[CuCl_4]^{3-}$, while Brugger et al. (2007) interpreted these spectral variations as geometric structural modifications of the $[CuCl_3]^{2-}$ complex induced by salt incorporation, emphasizing the instability of $[CuCl_4]^{3-}$ in solution. Sherman (2007) further substantiated through thermodynamic calculations that this species can not maintain stability in aqueous solutions at ambient conditions. Raman spectroscopic investigations by Applegarth et al. (2014) on the CuCl-HCl system (24–80 °C) revealed no characteristic peaks attributable to $[CuCl_4]^{3-}$ even at HCl concentrations up to 6 m, detecting only a Raman signature of $[CuCl_3]^{2-}$ near 240 cm^{-1}. Experimental results from our study conducted across an extended temperature range (24–300 °C) on the Cu-HCl system validate this conclusion, exclusively identifying a Raman characteristic peak at 235 cm^{-1} (represents $[CuCl_3]^{2-}$). This observation aligns with Brugger et al. (2007)'s XANES spectral interpretaions and Sherman (2007)'s thermodynamic modeling, collectively demonstrating that $[CuCl_4]^{3-}$ lacks thermodynamic stability even under elevated temperatures (< 300 °C) and high HCl concentrations (6 m).

4.1.2 Divalent copper (Cu^{2+}) species

Experimental studies employing electronic spectroscopy and XAS have demonstrated that under low-temperature (≤ 75 °C) and low-chloride (Cl ≤ 2 m) conditions, Cu^{2+} predominantly exists as the hydrated ion $[Cu(H_2O)_n]^{2+}$ (Collings et al. 2000; Brugger et al. 2001; Zhang et al. 2014, 2017). As summarized in Table 2, previous Raman spectroscopy studies assigned the characteristic peak at 440 cm^{-1} to the Cu–O stretching mode of the hydrated ion $[Cu(H_2O)_n]^{2+}$ (Hester and Planes 1964; Davis and Chong 1972). In our experiments, a weak peak at 440 cm^{-1} was observed in the 1 m $CuCl_2$ solution between 24 and 50 °C, which disappeared entirely at 100 °C. This indicates that the species represented by C_{440} exists only under low-temperature (< 100 °C) and low-chloride (Cl ≤ 2 m) conditions. Based on prior findings, we attribute the 440 cm^{-1} Raman peak to the Cu–O stretching vibration of $[Cu(H_2O)_n]^{2+}$ complex.

Under low-chloride conditions (Cl ≤ 2 m) and higher temperatures (> 100 °C), Trevani et al. (2010) identified $[CuCl_4]^{2-}$ as the dominant species at 150 °C using UV–Vis spectroscopy. Collings et al. (2000) inferred through EXAFS spectroscopy that $[CuCl]^+$ and $[CuCl_2]^0$ became predominant at 175 °C. Li et al. (2015) combined density functional theory and molecular dynamics simulations to propose that

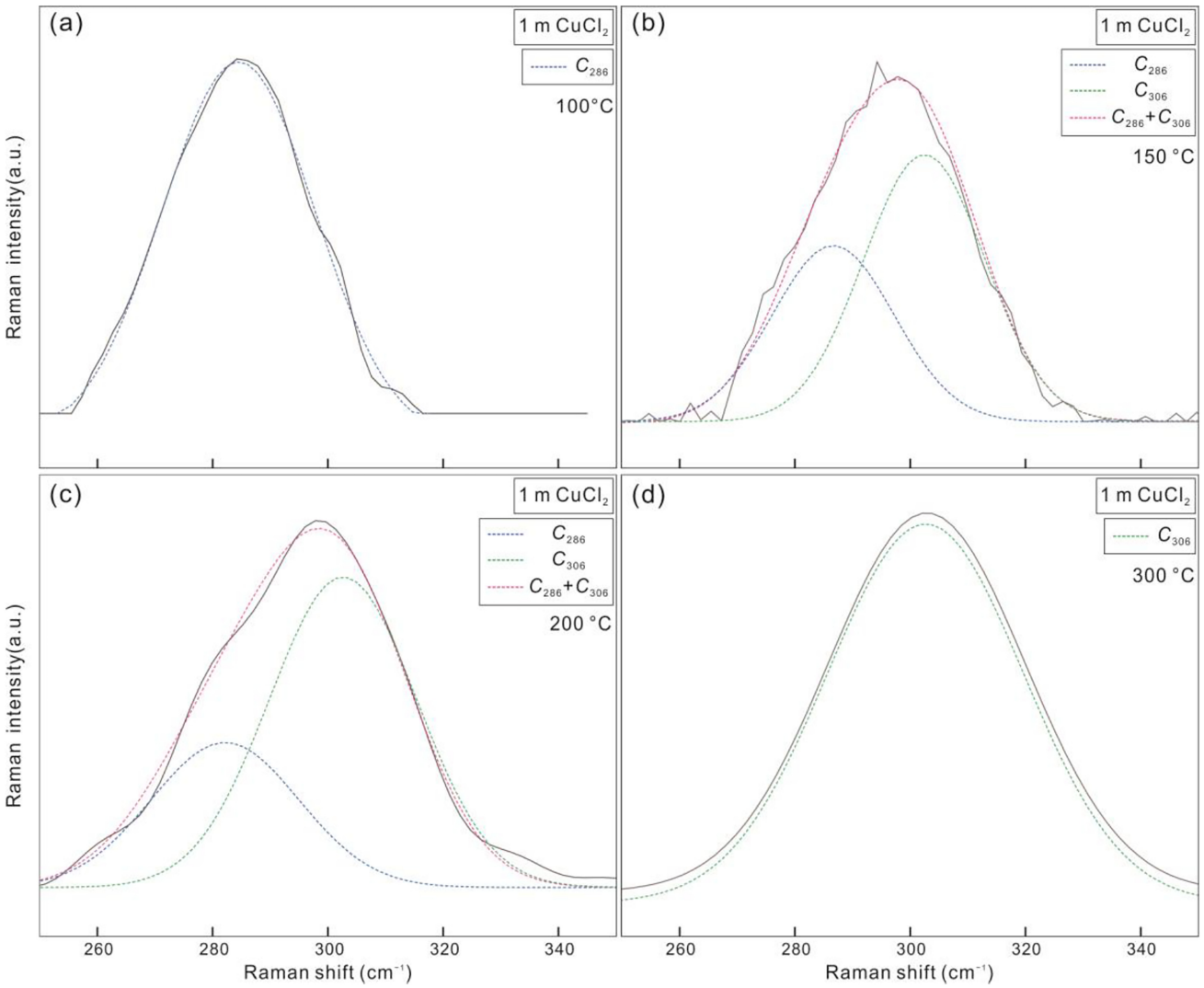

Fig. 7 Raman spectra of 1 m $CuCl_2$ solution at 100–300 °C (solid line represents the original spectrum, dashed line represents the peak fitting results of Peak software, with a confidence level of 99%)

$[CuCl_4]^{2-}$ stability decreases with rising temperature. Systematic Raman studies on Cu^{2+} chloride complexes remain limited, though tentative assignments suggest that the peak in the 280–286 cm^{-1} range may correspond to tetrahedrally coordinated Cu–Cl stretching modes in $[CuCl_4]^{2-}$, while broader features in 200–340 cm^{-1} could represent Cu–Cl stretching modes of other Cu^{2+} chloride (Tanimizu et al. 2007; Yang and Xu 2011; Wu et al. 2016). In our experiments with 1 m $CuCl_2$, a new peak emerged at 286 cm^{-1} at 50 °C. With increasing temperature, this peak shifted to higher wavenumbers, reaching 306 cm^{-1} at 300 °C. While thermal red shifts (low wavenumber shifts) typically arise from bond expansion or weakening (e.g., observed in Cu^{+}–Cl systems in this study) (Gu et al. 2007), the pronounced blue shift (286 cm^{-1} to 306 cm^{-1}) in the Cu^{2+}–Cl system likely reflects speciation changes. Peak fitting of Raman spectra from 100 to 300 °C using PeakFit software (Fig. 7) revealed that the C_{286} peak area dominated at 100 °C but progressively diminished with heating, while the C_{306} peak area increased, becoming dominant at 300 °C. This indicates a temperature-driven transition from C_{286}- to C_{306}-associated species. Integrating previous experimental findings and proposed Raman peak assignments (Table 2), we propose C_{286} observed at 50 °C corresponds to the tetrahedrally coordinated Cu–Cl stretching modes in $[CuCl_4]^{2-}$, and C_{306} observed at 300 °C likely represents Cu–Cl stretching modes of $[CuCl]^{+}$ and $[CuCl_2]^{0}$, which stabilize at high temperatures. This interpretation aligns with previous speciation models and resolves the anomalous blue shift through a temperature-dependent speciation mechanism.

4.2 Migration patterns of copper in medium- to low-temperature hydrothermal fluids and their connection with mineralization

In medium- to low-temperature hydrothermal systems, the precipitation and enrichment of copper are primarily controlled by decreasing chloride concentration, temperature, oxygen fugacity, and increasing pH. Part 2 of this study explores the effects of HCl concentration, temperature, and oxygen fugacity on copper transport mechanisms. Our experimental results demonstrate that higher HCl concentrations enhance Cu^+ coordination with Cl^-, stabilizing the higher-order complex $[CuCl_3]^{2-}$ under low-temperature and high-salinity conditions. The concurrent increase in Raman intensity and peak area of $[CuCl_3]^{2-}$ with rising HCl concentration indicates elevated dissolved copper levels in the solution. Temperature reduction drives a speciation shift from $[CuCl_2]^-$ to $[CuCl_3]^{2-}$, accompanied by decreased copper solubility and precipitation (Fig. 4d). Thermodynamic calculations (Xiao et al. 1998; Liu et al. 2002; Brugger et al. 2007) suggest that the destabilization of $[CuCl_2]^-$ during cooling critically impacts copper solubility. In our HCl system, crystalline precipitation observed during cooling from 350 to 300 °C (Fig. 4d) directly reflects this temperature-induced solubility decline. Oxygen fugacity reduction via hydrogen addition in Cu^{2+}–Cl reduction experiments triggered complete conversion to Cu^+–Cl complexes, yielding transparent crystals (Fig. 5b) (hypothesized to be CuCl solids). This highlights how shifts in copper oxidation state—such as mixing oxidized fluids with reducing agents or interaction of oxidized fluids with copper-bearing minerals (Hua et al. 2004; Chaudhari et al. 2021)—directly reduce solubility, driving copper precipitation. These findings collectively illustrate how coupled physicochemical conditions (T, fO_2) and fluid composition (Cl^-) govern copper behavior in hydrothermal systems.

Our study also investigates the phenomenon of reversible temperature-dependent changes in copper oxidation states within systems containing H^+ and SO_4^{2-} under low-temperature conditions (< 200 ℃). Mavrogenes et al. (2002) conducted XANES spectroscopy on copper-bearing fluid and vapor inclusions from the Mole Granite (New South Wales, Australia), revealing speciation shifts: $[Cu(H_2O)_6]^{2+}$ dominates at 25 ℃, transitioning to $[CuCl_2]^-$ at 200 ℃, and further to $[CuCl_2]^-$ or $[CuCl(H_2O)]^0$ near the liquid–vapor homogenization temperature (~ 400 ℃). They hypothesized that SO_4^{2-} and H^+ induce low-temperature oxidation of Cu^+ to Cu^{2+}, generating Cu minerals and acid alteration. Berry et al. (2006) observed similar reversible $Cu^+ \rightarrow Cu^{2+}$ oxidation in low-temperature $K^+/H^+/Cl^-$-bearing fluid inclusions using XANES. In contrast, our study of a $Cu^+/H^+/Cl^-$ system (1 m $CuCl_2 + H_2$) shows that Cu^+–Cl complexes remain dominant from 24 to 300 ℃, with no detectable Cu^{2+}–H_2O or Cu^{2+}–Cl complexes. Spectra collected after ≥ 24 h stabilization at 300 ℃ and room temperature exclude effects from H_2 or speciation instability. The $Cu^+/Cl^-/SO_4^{2-}/SO_2$ system (0.47 m $CuCl_2$ + 0.1 m $K_2S_2O_3$) yields analogous results: no changes in Cu oxidation state or Raman intensities of sulfur species during cooling, with Cu^+–Cl complexes persisting stably at room temperature.

Comparative analysis reveals that discrepancies in copper valence states between previous experimental results, and our findings may not only stem from differences in experimental systems but also relate to x-ray beam-induced redox effects. For instance, Mesu et al. (2005) demonstrated that prolonged x-ray beam exposure reduces Cu^{2+} to Cu^+, particularly pronounced in chloride-containing solutions. Brugger et al. (2007) observed similar phenomena during XAS of Cu^{2+}-bearing chloride solutions heated from 70 to 150 ℃: at 70 ℃, the system contained 76% Cu^{2+} and 24% Cu^+, while at 150 ℃, no detectable Cu^{2+} remained. These findings suggest that x-ray absorption spectroscopy may yield inaccurate assessments of copper oxidation states because of unavoidable beam-induced redox artifacts. Notably, however, Brugger et al. (2007) found that beam damage at elevated temperatures actually stabilizes Cu^+ in solution, thereby not interfering with studies of Cu^+ complexes. In Raman spectroscopic analyses, laser heating effects could perturb system temperatures (Hagiwara et al. 2021). To mitigate this, we systematically repositioned the laser beam after each spectral acquisition, minimizing thermal interference and enhancing result reliability. Our experimental data confirm that Cu^+–Cl complexes persist across a broad temperature range (low to high temperatures), actively participating in copper mineralization processes. This aligns with recent experimental work demonstrating that cuprous chloride complexes ($[CuCl_2]^-$, $[CuCl_3]^{2-}$) contribute significantly to the transport of copper in ore-forming hydrothermal fluids (e.g., red-bed copper deposits; Rose 1976) and hydrothermal overprinting of ore deposits (Zhang et al. 2021) under low-temperature reducing conditions.

5 Conclusion

This study employs fused silica capillary capsule coupled with in situ Raman spectroscopy to systematically acquire Raman spectra of copper-bearing hydrothermal fluids under saturated vapor pressure conditions (24–300 °C) across varying HCl concentrations (1–6 m) and redox environments ($H_2/K_2S_2O_3$-regulated systems). By analyzing characteristic peaks of Cu–Cl and Cu–O stretching vibrations (200 to 450 cm^{-1}), we elucidate the transport mechanisms of copper in hydrothermal fluids and the factors governing dissolution-precipitation dynamics:

(1) In reductive acidic systems, Cu^{+}–Cl complexes exhibit pronounced temperature-concentration dependence: under high-temperature conditions (> 200 °C), $[CuCl_2]^-$ emerges as the predominant species, with its proportion increasing with rising temperature. In low-temperature (<150 °C) and high Cl^- concentration (>2 m) systems, the proportion of $[CuCl_3]^{2-}$ becomes significantly enhanced, demonstrating stability positively correlated with Cl^- concentration. Notably, Cu^{+}–Cl complexes remain stable at room temperature, indicating their potential transport capacity in supergene environments.

(2) In oxidative acidic systems, the chloride speciation of Cu^{2+} also exhibits temperature-dependent evolution. At 300 °C, $[CuCl]^+$ and $[CuCl_2]^0$ are hypothesized to dominate. With decreasing temperature, the proportion of higher-coordination complexes such as $[CuCl_4]^{2-}$ increases, while below 50 °C, hydrated species like $[Cu(H_2O)_n]^{2+}$ may emerge. Through the introduction of H_2 and $K_2S_2O_3$, the reduction of $Cu^{2+}\rightarrow Cu^{+}$ was achieved. This process enables the detection of Cu^{+}–Cl complexes in the system, accompanied by copper precipitation triggered by reduced solubility.

(3) Precipitation control mechanism: Temperature decreasing directly destabilizes Cu–Cl complexes, inducing copper supersaturation and precipitation. Meanwhile, reductant addition (e.g., H_2) triggers copper valence transition ($Cu^{2+}\rightarrow Cu^{+}$) by lowering oxygen fugacity (fO_2), concurrently driving precipitation. Thus, during the evolution of geological fluids, variations in temperature, chloride concentration, and redox conditions critically govern copper dissolution, transport, and enrichment in hydrothermal systems, ultimately shaping its mineralization processes and diverse copper-bearing sulfides.

Acknowledgements This work is jointly funded by the Strategic Priority Research Program of the Chinese Academy of Sciences (grant No. XDA0430301) and the National Natural Science Foundation of China (grant Nos. 42130109, 41973059). The authors appreciate the reviewers for their constructive comments and suggestions, which significantly helped us improve our manuscript.

Author contributions ZW: conceptualization, formal analysis, resources, data curation; software (data process); writing—original draft, validation, visualization; LS (Corresponding author): validation, supervision, writing—reviewing and editing, funding acquisition; IC: supervision; writing—reviewing and editing; CC: writing—reviewing and editing; YZ: writing—reviewing and editing; JL: writing—reviewing and editing; ZJ: writing—reviewing and editing; XG: writing—reviewing and editing; YW: writing—reviewing and editing.

Funding This work is jointly funded by the Strategic Priority Research Program of the Chinese Academy of Sciences (grant No. XDA0430301) and the National Natural Science Foundation of China (grant Nos. 42130109, 41973059).

Data availability Data available on request from the authors.

Declarations

Conflict of interest The authors declare that they have no known competing financial interests or personal relationships that could influence the work presented in this paper.

Ethical approval N/A.

Consent The Author hereby grants the full and exclusive rights to the manuscript, all revisions, and the full copyright. The rights include but are not limited to the following: (1) to reproduce, publish, sell, and distribute copies of the manuscript, selections of the manuscript, and translations and other derivative works based upon the manuscript, in print, audio-visual, electronic, or by any and all media now or hereafter known or devised; (2) to license reprints of the manuscript to third persons for educational photocopying; (3) to license others to create abstracts of the manuscript and to index the manuscript; (4) to license secondary publishers to reproduce the manuscript in print, microform, or any computer-readable form, including electronic on-line databases; and (5) to license the manuscript for document delivery. These exclusive rights run the full term of the copyright, and all renewals and extensions thereof.

References

Applegarth LMSGA, Corbeil CR, Mercer DJW, Pye CC, Tremaine PR (2014) Raman and ab initio investigation of aqueous Cu(I) chloride complexes from 25 to 80 ℃. J Phys Chem B 118(1):204–214. https://doi.org/10.1021/jp406580q

Axtell DD, Good BW, Porterfield WW, Yoke JT (1973) Fused salts at room temperature. Vibrational spectroscopic and other studies of liquid chlorocuprates(I). J Am Chem Soc 95(14):4555–4559. https://doi.org/10.1021/ja00795a016

Berger JM, Winand R (1984) Solubilities, densities and electrical conductivities of aqueous copper(I) and copper(II) chlorides in solutions containing other chlorides such as iron, zinc, sodium and hydrogen chlorides. Hydrometallurgy 12(1):61–81. https://doi.org/10.1016/0304-386X(84)90048-3

Berry AJ, Hack AC, Mavrogenes JA, Newville M, Sutton SR (2006) A XANES study of Cu speciation in high-temperature brines using synthetic fluid inclusions. Am Mineral 91(11–12):1773–1782. https://doi.org/10.2138/am.2006.1940

Berry AJ, Harris AC, Kamenetsky VS, Newville M, Sutton SR (2009) The speciation of copper in natural fluid inclusions at temperatures up to 700 ℃. Chem Geol 259(1–2):2–7. https://doi.org/10.1016/j.chemgeo.2008.10.018

Brugger J, McPhail DC, Black J, Spiccia L (2001) Complexation of metal ions in brines: application of electronic spectroscopy in the study of the Cu(II)-LiCl-H_2O system between 25 and 90 °C. Geochim Cosmochim Acta 65(16):2691–2708. https://doi.org/10.1016/S0016-7037(01)00614-7

Brugger J, Etschmann B, Liu W, Testemale D, Hazemann JL, Emerich H, van Beek W, Proux O (2007) An XAS study of the structure and thermodynamics of Cu(I) chloride complexes in brines up to high temperature (400 °C, 600 bar). Geochim Cosmochim Acta 71(20):4920–4941. https://doi.org/10.1016/j.gca.2007.08.003

Chaudhari A, Webster NAS, Xia F, Frierdich A, Ram R, Etschmann B, Liu WH, Wykes J, Brand HEA, Brugger J (2021) Anatomy of a complex mineral replacement reaction: role of aqueous redox, mineral nucleation, and ion transport properties revealed by an in situ study of the replacement of chalcopyrite by copper sulfides. Chem Geol 581:120390. https://doi.org/10.1016/j.chemgeo.2021.120390

Chou IM, Song YC, Burruss RC (2008) A new method for synthesizing fluid inclusions in fused silica capillaries containing organic and inorganic material. Geochim Cosmochim Acta 72(21):5217–5231. https://doi.org/10.1016/j.gca.2008.07.030

Chou IM, Wang R, Fang J (2021) In situ redox control and Raman spectroscopic characterisation of solutions below 300 ℃. Geochem Persp Let 20:1–5. https://doi.org/10.7185/geochemlet.2135

Collings MD, Sherman DM, Ragnarsdottir KV (2000) Complexation of Cu^{2+} in oxidized NaCl brines from 25 ℃ to 175 ℃: results from in situ EXAFS spectroscopy. Chem Geol 167(1–2):65–73. https://doi.org/10.1016/s0009-2541(99)00200-4

Creighton JA, Lippincott ER (1963) 983. Raman spectra and solvent-extractions of cuprous halides. J Chem Soc. https://doi.org/10.1039/jr9630005134

Davis AR, Chong C (1972) Laser Raman study of aqueous copper nitrate solutions. Inorg Chem 11(8):1891–1895. https://doi.org/10.1021/ic50114a031

Fujii T, Moynier F, Abe M, Nemoto K, Albarède F (2013) Copper isotope fractionation between aqueous compounds relevant to low temperature geochemistry and biology. Geochim Cosmochim Acta 110:29–44. https://doi.org/10.1016/j.gca.2013.02.007

Gu MX, Pan LK, Tay BK, Sun CQ (2007) Atomistic origin and temperature dependence of Raman optical redshift in nanostructures: a broken bond rule. J Raman Spectrosc 38(6):780–788. https://doi.org/10.1002/jrs.1683

Hagiwara Y, Yoshida K, Yoneda A, Torimoto J, Yamamoto J (2021) Experimental variable effects on laser heating of inclusions during Raman spectroscopic analysis. Chem Geol 559:119928. https://doi.org/10.1016/j.chemgeo.2020.119928

Hester RE, Plane RA (1964) A Raman spectrophotometric comparison of interionic association in aqueous solutions of metal nitrates, sulfates, and perchlorates. Inorg Chem 3(5):769–770. https://doi.org/10.1021/ic50015a037

Hua M, Xu ZW, Rao B, Lu XC, Huang SS, Zhu SP (2004) Geochemical simulation experiment and surface mineralogy study of reaction between pyrite and $CuCl_2$ brine. J Nanjing Uni (Nat Sci) 03:279–286 (**in Chinese with English abstract**)

Hurai V, Huraiová M, Slobodník M, Thomas R (2015) Geofluids: developments in microthermometry, spectroscopy, thermodynamics, and stable isotopes. Elsevier press, Netherlands

Jianu OA, Wang ZL, Naterer GF, Rosen MA (2018) Constituent solubility and dissolution in a CuCl–HCl–H_2O ternary system. Chem Eng Sci 184:209–215. https://doi.org/10.1016/j.ces.2018.03.004

Li HJ, Yi HB, Xu JJ (2015) High-order Cu(II) chloro-complexes in LiCl brines: insights from density function theory and molecular dynamics. Geochim Cosmochim Acta 165:1–13. https://doi.org/10.1016/j.gca.2015.05.018

Liu WH, McPhail DC, Brugger J (2001) An experimental study of copper(I)-chloride and copper(I)-acetate complexing in hydrothermal solutions between 50 °C and 250 °C and vapor-saturated pressure. Geochim Cosmochim Acta 65(17):2937–2948. https://doi.org/10.1016/S0016-7037(01)00631-7

Liu WH, Brugger J, McPhail DC, Spiccia L (2002) A spectrophotometric study of aqueous copper(I)–chloride complexes in LiCl solutions between 100 ℃ and 250 ℃. Geochim Cosmochim Acta 66(20):3615–3633. https://doi.org/10.1016/s0016-7037(02)00942-0

Mavrogenes JA, Berry AJ, Newville M, Sutton SR (2002) Copper speciation in vapor-phase fluid inclusions from the Mole Granite, Australia. Am Mineral 87(10):1360–1364. https://doi.org/10.2138/am-2002-1011

Mesu JG, van der Eerden AMJ, de Groot FMF, Weckhuysen BM (2005) Synchrotron radiation effects on catalytic systems As probed with a combined in situ UV–vis/XAFS spectroscopic setup. J Phys Chem B 109(9):4042–4047. https://doi.org/10.1021/jp045206r

Rickard D, Cowper M (1994) Kinetics and mechanism of chalcopyrite formation from Fe(II) disulphide in aqueous solution (<200 °C). Geochim Cosmochim Acta 58(18):3795–3802. https://doi.org/10.1016/0016-7037(94)90364-6

Rose AW (1976) The effect of cuprous chloride complexes in the origin of red-bed copper and related deposits. Econ Geol 71(6):1036–1048. https://doi.org/10.2113/gsecongeo.71.6.1036

Schmidt C, Watenphul A, Jahn S, Schäpan I, Scholten L, Newville MG, Lanzirotti A (2018) Copper complexation and solubility in high-temperature hydrothermal fluids: a combined study by Raman, X-ray fluorescence, and X-ray absorption spectroscopies and ab initio molecular dynamics simulations. Chem Geol 494:69–79. https://doi.org/10.1016/j.chemgeo.2018.07.018

Scholz B, Lüdemann HD, Franck EU (1972) Spectra of Cu(II)-complexes in aqueous solutions at high temperatures and pressures. Ber Bunsenges Phys Chem 76(5):406–409. https://doi.org/10.1002/bbpc.19720760508

Sherman DM (2007) Complexation of Cu+ in hydrothermal NaCl brines: Ab initio molecular dynamics and energetics. Geochim Cosmochim Acta 71(3):714–722. https://doi.org/10.1016/j.gca.2006.09.015

Stoicheff B (1957) High resolution Raman spectroscopy of gases: IX. spectra of H_2, HD, and D_2. Can J Phys 35(6):730–741. https://doi.org/10.1139/p57-079

Tanimizu M, Takahashi Y, Nomura M (2007) Spectroscopic study on the anion exchange behavior of Cu chloro-complexes in HCl Solutions and its implication to Cu isotopic fractionation. Geochem J 41(4):291–295. https://doi.org/10.2343/geochemj.41.291

Trevani L, Ehlerova J, Sedlbauer J, Tremaine PR (2010) Complexation in the Cu(II)–LiCl–H_2O system at temperatures to 423 K by UV-Visible spectroscopy. Int J Hydrog Energy 35(10):4893–4900. https://doi.org/10.1016/j.ijhydene.2009.10.046

Wu XJ, Yu XH, Liu AZ, Jiang WG, Chen LJ (2016) Study on $CuCl_2$ in aqueous solutions by density functional theory and Raman spectroscopy. Chemistry 79(8):754–759. https://doi.org/10.14159/j.cnki.0441-3776.2016.08.011. (**in Chinese with English abstractcc**)

Xiao ZF, Gammons CH, Williams-Jones AE (1998) Experimental study of copper(I) chloride complexing in hydrothermal solutions at 40 to 300 ℃ and saturated water vapor pressure. Geochim Cosmochim Acta 62(17):2949–2964. https://doi.org/10.1016/S0016-7037(98)00228-2

Yang D, Xu W (2011) Study on complexation Raman spectroscopy of $CuCl_2$–H_2O and $FeCl_3$–H_2O systems and exploration of solution Raman quantitative analysis. Spectr Spectral Anal 31(10):2742–2746. https://doi.org/10.3964/j.issn.1000-0593(2011)10-2742-05. (**in Chinese with English abstract**)

Zhang N, Zeng DW, Hefter G, Chen QY (2014) Chemical speciation in concentrated aqueous solutions of $CuCl_2$ using thin-film UV–visible spectroscopy combined with DFT calculations. J Mol Liq 198:200–203. https://doi.org/10.1016/j.molliq.2014.06.025

Zhang N, Wang WL, Brugger J, Zhang G, Zeng DW (2017) Species fine structure of transition metal Cu(II) in aqueous chloride-bearing solutions: insights from X-ray absorption spectroscopy and ab initio XANES calculations. J Mol Liq 230:200–208. https://doi.org/10.1016/j.molliq.2017.01.019

Zhang Y, Li WQ, Cai YF, Qu Y, Pan YG, Zhang WL, Zhao KD (2021) Experimental investigation of the reactions between pyrite and aqueous Cu(I) chloride solution at 100–250 °C. Geochim Cosmochim Acta 298:1–20. https://doi.org/10.1016/j.gca.2021.01.018